The Astronomical Journal, 135:1749–1756, 2008 May
doi:10.1088/0004-6256/135/5/1749

HIGH-PRECISION PHOTOMETRY OF EXTREME KBO 2003 EL_{61}

Pedro Lacerda[1], David Jewitt[1], and Nuno Peixinho[1,2]
[1] Institute for Astronomy, University of Hawaii, 2680 Woodlawn Drive, Honolulu, HI 96822, USA; pedro@ifa.hawaii.edu
[2] Grupo de Astrofísica, Universidade de Coimbra, Portugal
Received 2007 November 26; accepted 2008 January 25; published 2008 April 2

ABSTRACT

We present high-precision, time-resolved, visible and near-infrared photometry of the large (diameter $\sim$ 2500 km) Kuiper belt object (136108) 2003 EL_{61}. The new data confirm rapid rotation at period $P = 3.9155 \pm 0.0001$ h with a peak-to-peak photometric range of $\Delta m_R = 0.29 \pm 0.02$ mag and further show subtle but reproducible color variations with rotation. Rotational deformation of 2003 EL_{61} alone would give rise to a symmetric light curve free of color variations. The observed photometric deviations from the best-fit equilibrium model show the existence of a large surface region with an albedo and color different from the mean surface of 2003 EL_{61}. We explore constraints on the nature of this anomalous region set by the existing data.

Key words: Kuiper Belt – methods: data analysis – minor planets, asteroids – solar system: general – techniques: photometric

1. INTRODUCTION

The known Kuiper belt objects (KBOs) extend in size from bodies so small as to be at the limits of sensitivity of the largest telescopes up to Pluto-sized bodies large enough to have body shapes controlled by self-gravity. The large objects are particularly amenable to physical study and a number of intriguing results have already been secured. The case of Pluto is well known: the main object rotates slowly (period $\sim$6 days) but the massive satellite Charon carries enough angular momentum that the system as a whole is near the critical threshold for breakup (McKinnon 1989). Surface maps derived from mutual occultation events show a spatially variegated surface, with a wide range of local albedos (from 0.1 to 0.9: Buie et al. 1992; Young et al. 1999) that may be related to surface deposition of frosts from Pluto's thin atmosphere (Trafton 1989). Other KBOs have less well-known physical properties, but new data are beginning to reveal a startling range of surface types (Jewitt & Luu 2004; Tegler et al. 2007; Trujillo et al. 2007) and rotational (Lacerda & Luu 2006; Sheppard 2007) properties. Notable examples of the latter include $\sim$900 km diameter (20000) Varuna, whose 6 h period and 0.4 mag photometric range are best explained as products of a rotationally deformed body shape and a bulk density of 1000 kg m^{-3} (Jewitt & Sheppard 2002; Takahashi & Ip 2004; Lacerda & Jewitt 2007). The large amplitude (1.14 $\pm$ 0.04 mag), long rotation period (13.7744 $\pm$ 0.0004 h), and eclipsing binary-like light curve of $\sim$240 km diameter 2001 QG_{298} suggest an even more extreme interpretation as a contact or near-contact binary (Sheppard & Jewitt 2004; Lacerda & Jewitt 2007).

One of the most remarkable of the large KBOs yet to be identified is (136108) 2003 EL_{61} (hereafter "EL61"), whose rapid rotation (period $\sim$3.9154 $\pm$ 0.0002 h), light-curve range ($\Delta m_R \sim 0.4$ mag), and near-symmetric morphology together suggest a rotationally deformed body of density $\sim$2500 kg m^{-3} (Rabinowitz et al. 2006; Lacerda & Jewitt 2007). EL61 is further interesting in its own right, as an extreme example of a large KBO with a rapid spin and also as the possible parent of a reported dynamical cluster of KBOs, perhaps produced by an ancient, shattering collision (Brown et al. 2007; Ragozzine & Brown 2007). Some members of this dynamical cluster share spectral features with EL61. Nearly all Pluto-sized KBOs have methane rich surfaces. EL61 is unusual in that it is covered in almost pure crystalline H_2O ice (see Figure 1; Trujillo et al. 2007). In this paper, we present new high-precision, time-resolved photometry taken to further explore the nature of EL61.

2. OBSERVATIONS

Optical observations were taken using the 2.2 m diameter University of Hawaii telescope atop Mauna Kea, Hawaii. We used a Tektronix 2048×2048 pixel charge-coupled device (CCD) mounted at the f/10 Cassegrain focus, giving pixels each 0.219 arcsecond square. Observations were obtained through broadband *BVRI* filters approximating the Kron–Cousins photometric system. The data were instrumentally calibrated using bias frames and flat-field images obtained from dithered, median-combined images of the twilight sky. Photometric calibration was obtained from observations of standards PG1323-085C, 107 457, Markarian A1, and PG1633-099A from the list by Landolt (1992).

Near-infrared observations were taken using the 3.8 m diameter United Kingdom Infrared Telescope (UKIRT), also located on Mauna Kea. We used the UIST imaging camera, which houses a 1024×1024 pixel array having an image scale of 0.12 arcsec per pixel. Our principal aim was to use the near-infrared wavelengths to search for rotational variability of water ice on the surface of EL61. For this purpose, we elected to use two filters, one to measure the 1.5 μm band of water ice and the other to sample the reflected continuum. Use of two filters, as opposed to a near-infrared spectrometer, allowed us to maintain rapid sampling (important because of the short rotation period of EL61) and high signal-to-noise ratios. Given the available UKIRT filter set, we employed the "$CH4_s$" filter (center 1.60 μm, full width at half maximum (FWHM) = 0.11 μm) to measure the water band (see Figure 1). The Mauna Kea J-band filter (center 1.25 μm, FWHM = 0.16 μm) provided a suitable measure of the continuum. In the remainder of the text we refer to these filters as "1.6 μm" and "1.25 μm." Photometric calibration of the UKIRT data was obtained from observations of standard stars S791-C and S813-D from Persson et al. (1998). The flux through each filter was measured relative to a field star and a second star was used to verify the regularity of the first. Since simultaneous measurements through the 1.25 μm and 1.6 μm

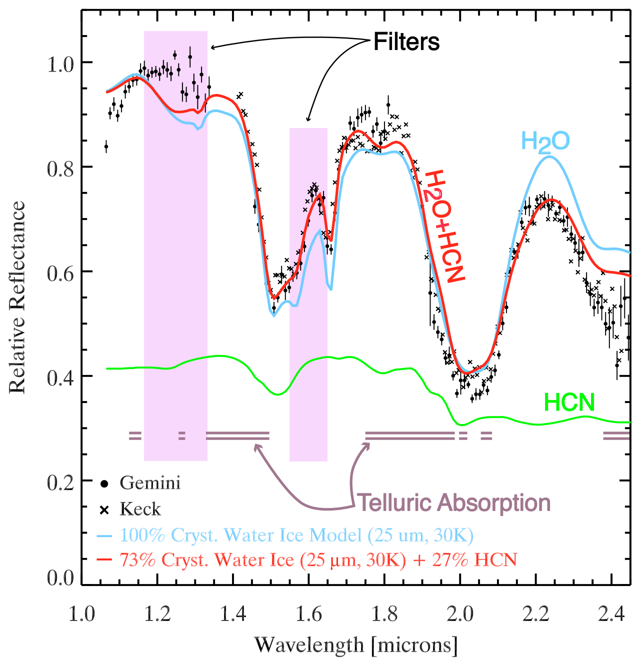

Figure 1. Near-IR spectrum of 2003 EL61, adapted from Trujillo et al. (2007). A pure crystalline water-ice model fit and a mix of water ice and HCN ice are overplotted. The locations and approximate widths of the 1.25 μm and 1.6 μm filters used to monitor the 1.5 μm water-ice band depth, as well as the wavelength regions where the Earth's atmosphere is opaque, are also shown.

Table 1
Journal of Observations

UT date	R[a] (AU)	Δ[b] (AU)	α[c] (°)	Tel.[d]	Filt.[e]	Seeing[f] ($''$)	Exp. time[g] (s)
2007 Jun 11	51.1570	50.8037	1.07	UH2.2m	R	0.9	80
2007 Jun 13	51.1567	50.8296	1.08	UH2.2m	R	1.0	80
2007 Jun 15	51.1565	50.8576	1.09	UH2.2m	B	0.9	260
2007 Jul 07	51.1536	51.1800	1.14	UKIRT	J	1.0	60
2007 Jul 08	51.1535	51.1949	1.14	UKIRT	J	1.2	60
2007 Jul 22	51.1517	51.4001	1.10	UH2.2m	B	1.5	300
2007 Jul 24	51.1514	51.4286	1.09	UH2.2m	B, R	1.5	260, 80

Notes.
[a] Heliocentric distance in AU.
[b] Geocentric distance in AU.
[c] Phase angle in degrees.
[d] Telescope used.
[e] Filters used.
[f] Typical seeing in arcseconds.
[g] Typical integration time per frame in seconds.

filters were not possible, we cross-interpolated their fluxes to the same times and measured the ratio of the interpolated values. A summarized journal of observations can be found in Table 1, and the final calibrated broadband photometric measurements are shown in Tables 2–4. Table 5 shows the ratio of flux density at 1.6 μm to the continuum flux density at 1.25 μm, as a function of time.

3. RESULTS AND DISCUSSION

Photometric measurements were obtained first relative to field stars to provide protection from transient changes in the transparency of the Earth's atmosphere and variations in the seeing (which can impact the accuracy of photometry obtained through

Table 2
B-band Photometry

UT date[a]	Julian date[a]	m_B[b]
2007 Jun 14.98390	2454266.483896	18.169 ± 0.005
2007 Jun 14.98989	2454266.489892	18.192 ± 0.005
2007 Jun 15.00129	2454266.501292	18.287 ± 0.005
2007 Jun 15.00572	2454266.505724	18.329 ± 0.005
2007 Jun 15.00999	2454266.509995	18.370 ± 0.005
2007 Jun 15.01429	2454266.514289	18.397 ± 0.005
2007 Jun 15.01869	2454266.518686	18.403 ± 0.005
2007 Jun 15.03386	2454266.533860	18.363 ± 0.005
2007 Jun 15.03757	2454266.537575	18.337 ± 0.005
2007 Jun 15.04263	2454266.542632	18.288 ± 0.005
2007 Jun 15.04688	2454266.546879	18.235 ± 0.005
2007 Jun 15.05056	2454266.550560	18.192 ± 0.005
2007 Jun 15.05445	2454266.554448	18.166 ± 0.005
2007 Jun 15.05819	2454266.558186	18.135 ± 0.005
2007 Jun 15.06184	2454266.561844	18.114 ± 0.005
2007 Jun 15.06554	2454266.565535	18.104 ± 0.005
2007 Jun 15.06924	2454266.569239	18.116 ± 0.005
2007 Jun 15.07287	2454266.572872	18.122 ± 0.005
2007 Jun 15.07658	2454266.576576	18.148 ± 0.005
2007 Jun 15.08022	2454266.580221	18.166 ± 0.005
2007 Jun 15.08414	2454266.584144	18.209 ± 0.005
2007 Jun 15.08831	2454266.588311	18.263 ± 0.005
2007 Jun 15.09185	2454266.591852	18.283 ± 0.005
2007 Jun 15.09541	2454266.595405	18.315 ± 0.005
2007 Jun 15.09896	2454266.598958	18.328 ± 0.005
2007 Jun 15.10251	2454266.602511	18.348 ± 0.005
2007 Jun 15.10633	2454266.606329	18.356 ± 0.005
2007 Jun 15.10989	2454266.609894	18.347 ± 0.005
2007 Jun 15.11345	2454266.613448	18.343 ± 0.005
2007 Jun 15.11699	2454266.616988	18.329 ± 0.005
2007 Jun 15.12054	2454266.620541	18.320 ± 0.005
2007 Jun 15.12433	2454266.624326	18.295 ± 0.005
2007 Jun 15.12788	2454266.627878	18.261 ± 0.005
2007 Jun 15.13144	2454266.631443	18.225 ± 0.005
2007 Jun 15.13499	2454266.634995	18.202 ± 0.005
2007 Jun 15.13855	2454266.638549	18.184 ± 0.005
2007 Jun 15.14281	2454266.642808	18.161 ± 0.005
2007 Jul 22.96857	2454304.468573	18.325 ± 0.007
2007 Jul 22.97550	2454304.475497	18.283 ± 0.007
2007 Jul 22.98246	2454304.482463	18.221 ± 0.007
2007 Jul 22.98775	2454304.487747	18.183 ± 0.007
2007 Jul 22.99173	2454304.491731	18.177 ± 0.007
2007 Jul 22.99578	2454304.495777	18.177 ± 0.007
2007 Jul 23.00453	2454304.504533	18.215 ± 0.007
2007 Jul 23.00859	2454304.508593	18.238 ± 0.007
2007 Jul 23.01263	2454304.512634	18.288 ± 0.007
2007 Jul 23.01670	2454304.516700	18.328 ± 0.007
2007 Jul 23.02072	2454304.520717	18.349 ± 0.007
2007 Jul 23.02722	2454304.527220	18.388 ± 0.007
2007 Jul 23.03125	2454304.531245	18.410 ± 0.007
2007 Jul 24.97186	2454306.471861	18.283 ± 0.014
2007 Jul 24.97540	2454306.475403	18.333 ± 0.014
2007 Jul 24.98242	2454306.482416	18.360 ± 0.014
2007 Jul 24.98596	2454306.485957	18.389 ± 0.014
2007 Jul 24.99282	2454306.492821	18.400 ± 0.014
2007 Jul 24.99636	2454306.496361	18.394 ± 0.014
2007 Jul 25.00914	2454306.509139	18.326 ± 0.014
2007 Jul 25.01268	2454306.512680	18.269 ± 0.014
2007 Jul 25.01957	2454306.519566	18.233 ± 0.014
2007 Jul 25.02311	2454306.523107	18.191 ± 0.014
2007 Jul 25.03137	2454306.531371	18.108 ± 0.014

Notes.
[a] Dates are light-time corrected.
[b] Apparent magnitude.

Table 3
R-band Photometry

UT date[a]	Julian date[a]	m_R[b]
2007 Jun 10.96450	2454262.464497	17.314 ± 0.009
2007 Jun 10.96670	2454262.466696	17.293 ± 0.009
2007 Jun 10.96809	2454262.468085	17.280 ± 0.009
2007 Jun 10.97004	2454262.470041	17.263 ± 0.009
2007 Jun 10.97143	2454262.471430	17.249 ± 0.009
2007 Jun 10.97282	2454262.472819	17.237 ± 0.009
2007 Jun 10.97491	2454262.474913	17.212 ± 0.009
2007 Jun 10.97637	2454262.476371	17.190 ± 0.009
2007 Jun 10.97782	2454262.477818	17.188 ± 0.009
2007 Jun 10.97930	2454262.479299	17.176 ± 0.009
2007 Jun 10.98076	2454262.480758	17.160 ± 0.009
2007 Jun 11.00040	2454262.500399	17.193 ± 0.009
2007 Jun 11.00186	2454262.501856	17.195 ± 0.009
2007 Jun 11.00330	2454262.503303	17.209 ± 0.009
2007 Jun 11.00476	2454262.504761	17.223 ± 0.009
2007 Jun 11.00622	2454262.506220	17.244 ± 0.009
2007 Jun 11.00823	2454262.508233	17.260 ± 0.009
2007 Jun 11.00969	2454262.509692	17.281 ± 0.009
2007 Jun 11.01115	2454262.511149	17.281 ± 0.009
2007 Jun 11.01260	2454262.512596	17.305 ± 0.009
2007 Jun 11.01404	2454262.514043	17.315 ± 0.009
2007 Jun 11.01580	2454262.515802	17.328 ± 0.009
2007 Jun 11.01727	2454262.517272	17.328 ± 0.009
2007 Jun 11.01873	2454262.518730	17.330 ± 0.009
2007 Jun 11.02018	2454262.520176	17.360 ± 0.009
2007 Jun 11.02162	2454262.521623	17.354 ± 0.009
2007 Jun 11.02323	2454262.523232	17.365 ± 0.009
2007 Jun 11.02468	2454262.524678	17.368 ± 0.009
2007 Jun 11.02615	2454262.526148	17.371 ± 0.009
2007 Jun 11.02761	2454262.527607	17.373 ± 0.009
2007 Jun 11.02905	2454262.529052	17.378 ± 0.009
2007 Jun 11.03132	2454262.531321	17.381 ± 0.009
2007 Jun 11.03277	2454262.532768	17.373 ± 0.009
2007 Jun 11.03423	2454262.534226	17.365 ± 0.009
2007 Jun 11.03570	2454262.535696	17.381 ± 0.009
2007 Jun 11.03714	2454262.537143	17.367 ± 0.009
2007 Jun 11.06471	2454262.564711	17.194 ± 0.009
2007 Jun 11.06617	2454262.566169	17.182 ± 0.009
2007 Jun 11.06763	2454262.567628	17.184 ± 0.009
2007 Jun 11.06913	2454262.569132	17.188 ± 0.009
2007 Jun 11.07058	2454262.570579	17.188 ± 0.009
2007 Jun 11.07210	2454262.572095	17.193 ± 0.009
2007 Jun 11.07355	2454262.573553	17.197 ± 0.009
2007 Jun 11.07500	2454262.574999	17.198 ± 0.009
2007 Jun 11.07646	2454262.576458	17.213 ± 0.009
2007 Jun 11.07792	2454262.577916	17.225 ± 0.009
2007 Jun 11.08353	2454262.583529	17.270 ± 0.009
2007 Jun 11.08499	2454262.584988	17.274 ± 0.009
2007 Jun 11.08643	2454262.586434	17.293 ± 0.009
2007 Jun 11.08789	2454262.587892	17.307 ± 0.009
2007 Jun 11.08934	2454262.589339	17.309 ± 0.009
2007 Jun 11.09200	2454262.592001	17.356 ± 0.009
2007 Jun 11.09346	2454262.593459	17.364 ± 0.009
2007 Jun 11.09493	2454262.594929	17.366 ± 0.009
2007 Jun 11.09637	2454262.596375	17.408 ± 0.009
2007 Jun 11.09783	2454262.597833	17.389 ± 0.009
2007 Jun 11.09978	2454262.599777	17.410 ± 0.009
2007 Jun 11.10124	2454262.601236	17.419 ± 0.009
2007 Jun 11.10272	2454262.602717	17.412 ± 0.009
2007 Jun 11.10419	2454262.604187	17.419 ± 0.009
2007 Jun 11.10563	2454262.605633	17.425 ± 0.009
2007 Jun 11.10780	2454262.607797	17.430 ± 0.009
2007 Jun 11.10924	2454262.609244	17.422 ± 0.009
2007 Jun 11.11070	2454262.610702	17.416 ± 0.009
2007 Jun 11.11216	2454262.612161	17.427 ± 0.009
2007 Jun 11.11361	2454262.613607	17.414 ± 0.009

Table 3
(Continued)

UT date[a]	Julian date[a]	m_R[b]
2007 Jun 11.11600	2454262.616002	17.413 ± 0.009
2007 Jun 11.11746	2454262.617461	17.386 ± 0.009
2007 Jun 11.11892	2454262.618919	17.360 ± 0.009
2007 Jun 11.12038	2454262.620377	17.384 ± 0.009
2007 Jun 11.12184	2454262.621836	17.367 ± 0.009
2007 Jun 11.12435	2454262.624347	17.359 ± 0.009
2007 Jun 11.12583	2454262.625828	17.338 ± 0.009
2007 Jun 11.12729	2454262.627286	17.331 ± 0.009
2007 Jun 11.12874	2454262.628744	17.316 ± 0.009
2007 Jun 11.13019	2454262.630191	17.296 ± 0.009
2007 Jun 11.13174	2454262.631742	17.267 ± 0.009
2007 Jun 11.13320	2454262.633200	17.255 ± 0.009
2007 Jun 11.13466	2454262.634658	17.239 ± 0.009
2007 Jun 11.13612	2454262.636116	17.229 ± 0.009
2007 Jun 11.14613	2454262.646127	17.154 ± 0.009
2007 Jun 11.14843	2454262.648430	17.144 ± 0.009
2007 Jun 11.14989	2454262.649888	17.141 ± 0.009
2007 Jun 11.15137	2454262.651370	17.137 ± 0.009
2007 Jun 11.15283	2454262.652828	17.138 ± 0.009
2007 Jun 11.15427	2454262.654274	17.143 ± 0.009
2007 Jun 11.15618	2454262.656183	17.140 ± 0.009
2007 Jun 11.15764	2454262.657642	17.151 ± 0.009
2007 Jun 11.15912	2454262.659123	17.160 ± 0.009
2007 Jun 12.96765	2454264.467647	17.291 ± 0.006
2007 Jun 12.97079	2454264.470795	17.309 ± 0.006
2007 Jun 12.97257	2454264.472566	17.336 ± 0.006
2007 Jun 12.97661	2454264.476606	17.344 ± 0.006
2007 Jun 12.97867	2454264.478666	17.362 ± 0.006
2007 Jun 12.98030	2454264.480298	17.369 ± 0.006
2007 Jun 12.98213	2454264.482126	17.351 ± 0.006
2007 Jun 12.98372	2454264.483723	17.390 ± 0.006
2007 Jun 12.98544	2454264.485436	17.390 ± 0.006
2007 Jun 12.98704	2454264.487044	17.384 ± 0.006
2007 Jun 12.98870	2454264.488700	17.390 ± 0.006
2007 Jun 12.99031	2454264.490308	17.386 ± 0.006
2007 Jun 12.99192	2454264.491917	17.390 ± 0.006
2007 Jun 12.99350	2454264.493502	17.370 ± 0.006
2007 Jun 12.99514	2454264.495145	17.363 ± 0.006
2007 Jun 12.99673	2454264.496731	17.367 ± 0.006
2007 Jun 12.99839	2454264.498386	17.356 ± 0.006
2007 Jun 12.99994	2454264.499937	17.359 ± 0.006
2007 Jun 13.00152	2454264.501523	17.335 ± 0.006
2007 Jun 13.00317	2454264.503165	17.332 ± 0.006
2007 Jun 13.00480	2454264.504797	17.325 ± 0.006
2007 Jun 13.00657	2454264.506568	17.305 ± 0.006
2007 Jun 13.00833	2454264.508327	17.288 ± 0.006
2007 Jun 13.00994	2454264.509936	17.268 ± 0.006
2007 Jun 13.01190	2454264.511904	17.251 ± 0.006
2007 Jun 13.01366	2454264.513662	17.248 ± 0.006
2007 Jun 13.01527	2454264.515271	17.229 ± 0.006
2007 Jun 13.01684	2454264.516845	17.221 ± 0.006
2007 Jun 13.01844	2454264.518442	17.202 ± 0.006
2007 Jun 13.02004	2454264.520039	17.196 ± 0.006
2007 Jun 13.02191	2454264.521914	17.195 ± 0.006
2007 Jun 13.02344	2454264.523441	17.189 ± 0.006
2007 Jun 13.02503	2454264.525027	17.181 ± 0.006
2007 Jun 13.02662	2454264.526624	17.182 ± 0.006
2007 Jun 13.02829	2454264.528290	17.189 ± 0.006
2007 Jun 13.08447	2454264.584469	17.329 ± 0.006
2007 Jun 13.08607	2454264.586065	17.301 ± 0.006
2007 Jun 13.08778	2454264.587778	17.292 ± 0.006
2007 Jun 13.08932	2454264.589318	17.267 ± 0.006
2007 Jun 13.09105	2454264.591054	17.264 ± 0.006
2007 Jun 13.09261	2454264.592605	17.230 ± 0.006
2007 Jun 13.09419	2454264.594190	17.222 ± 0.006
2007 Jun 13.09581	2454264.595810	17.198 ± 0.006

Table 3
(Continued)

UT date[a]	Julian date[a]	m_R[b]
2007 Jun 13.09750	2454264.597499	17.184 ± 0.006
2007 Jun 13.09912	2454264.599120	17.171 ± 0.006
2007 Jun 13.10073	2454264.600729	17.167 ± 0.006
2007 Jun 13.10237	2454264.602372	17.150 ± 0.006
2007 Jun 13.10396	2454264.603958	17.146 ± 0.006
2007 Jun 13.10552	2454264.605519	17.131 ± 0.006
2007 Jun 13.10723	2454264.607232	17.150 ± 0.006
2007 Jun 13.10886	2454264.608864	17.131 ± 0.006
2007 Jun 13.11044	2454264.610438	17.137 ± 0.006
2007 Jun 13.11207	2454264.612070	17.137 ± 0.006
2007 Jun 13.11370	2454264.613702	17.135 ± 0.006
2007 Jun 13.11525	2454264.615252	17.154 ± 0.006
2007 Jun 13.11692	2454264.616919	17.159 ± 0.006
2007 Jun 13.11848	2454264.618481	17.177 ± 0.006
2007 Jun 13.12009	2454264.620090	17.178 ± 0.006
2007 Jun 13.12168	2454264.621676	17.186 ± 0.006
2007 Jun 13.12326	2454264.623261	17.213 ± 0.006
2007 Jun 13.12490	2454264.624904	17.230 ± 0.006
2007 Jun 13.12654	2454264.626536	17.249 ± 0.006
2007 Jun 13.12817	2454264.628168	17.234 ± 0.006
2007 Jun 13.12981	2454264.629811	17.288 ± 0.006
2007 Jun 13.13143	2454264.631432	17.300 ± 0.006
2007 Jun 13.13302	2454264.633017	17.332 ± 0.006
2007 Jun 13.13459	2454264.634590	17.326 ± 0.006
2007 Jun 13.13633	2454264.636326	17.335 ± 0.006
2007 Jun 13.13789	2454264.637889	17.350 ± 0.006
2007 Jun 13.13942	2454264.639417	17.379 ± 0.006
2007 Jun 13.14119	2454264.641187	17.372 ± 0.006
2007 Jun 13.14290	2454264.642900	17.383 ± 0.006
2007 Jun 13.14458	2454264.644578	17.400 ± 0.006
2007 Jun 13.14623	2454264.646233	17.378 ± 0.005
2007 Jun 13.14793	2454264.647934	17.381 ± 0.005
2007 Jul 24.97919	2454306.479187	17.412 ± 0.005
2007 Jul 24.98065	2454306.480645	17.417 ± 0.005
2007 Jul 24.98979	2454306.489788	17.389 ± 0.005
2007 Jul 24.99123	2454306.491234	17.367 ± 0.005
2007 Jul 25.00570	2454306.505702	17.287 ± 0.005
2007 Jul 25.00717	2454306.507171	17.277 ± 0.005
2007 Jul 25.01650	2454306.516499	17.199 ± 0.005
2007 Jul 25.01795	2454306.517946	17.170 ± 0.005

Notes.
[a] Dates are light-time corrected.
[b] Apparent magnitude.

discrete apertures). The resulting measurements were calibrated against standard stars using large aperture photometry. The internal accuracy of the light-curve data in the B and R filters is good to about ±0.01 mag while, in the infrared, scatter in the photometry shows that the accuracy is at the ±0.03 mag level. We did not apply a phase angle correction to the data. The phase angle changed from 1.07° to 1.10° in our B and R observations. In this 0.03°phase angle range, with a phase coefficient of $\sim$0.1 mag deg^{-1} (Rabinowitz et al. 2007), the effect of phase is only 0.003 mag and therefore unimportant compared to the 0.01 mag photometric accuracy. Furthermore, the color dependence of the phase coefficient is small for EL61 according to these authors, and the expected change in the color resulting from phase angle is only about 0.001 mag, which is again negligible.

The best-fit light-curve period was determined from the R-band data using phase-dispersion minimization (PDM; Stellingwerf 1978) as $P = 3.9155 \pm 0.0001$ h (two-peaked light curve). This period is in close agreement with $P = 3.9154 \pm 0.0002$ h determined independently (Rabinowitz et al. 2006). Photometry in the other filters was scaled to the R-band light curve by subtracting the median colors $B - R = 0.972$ and $R - J = 0.88$, as determined from our data. The $B - R$ color is again in good agreement with $B - R = 0.969 \pm 0.030$ reported by Rabinowitz et al; these authors did not measure $R - J$.

Table 4
J-band Photometry

UT date[a]	Julian date[a]	m_J[b]
2007 Jul 6.97424	2454288.474241	16.50 ± 0.04
2007 Jul 6.98283	2454288.482830	16.47 ± 0.04
2007 Jul 6.99100	2454288.490998	16.38 ± 0.03
2007 Jul 6.99918	2454288.499178	16.33 ± 0.03
2007 Jul 7.00775	2454288.507750	16.29 ± 0.03
2007 Jul 7.01586	2454288.515861	16.31 ± 0.03
2007 Jul 7.02574	2454288.525740	16.42 ± 0.03
2007 Jul 7.03704	2454288.537044	16.55 ± 0.04
2007 Jul 7.04504	2454288.545038	16.57 ± 0.04
2007 Jul 7.05309	2454288.553091	16.55 ± 0.04
2007 Jul 7.06125	2454288.561255	16.49 ± 0.03
2007 Jul 7.06936	2454288.569363	16.41 ± 0.03
2007 Jul 7.07745	2454288.577448	16.32 ± 0.03
2007 Jul 7.98350	2454289.483504	16.27 ± 0.04
2007 Jul 7.99131	2454289.491311	16.28 ± 0.04
2007 Jul 7.99912	2454289.499119	16.34 ± 0.04
2007 Jul 8.00692	2454289.506925	16.44 ± 0.04
2007 Jul 8.02456	2454289.524560	16.54 ± 0.04
2007 Jul 8.03236	2454289.532361	16.55 ± 0.04
2007 Jul 8.04017	2454289.540167	16.47 ± 0.04
2007 Jul 8.04800	2454289.547996	16.42 ± 0.04
2007 Jul 8.05583	2454289.555835	16.33 ± 0.04
2007 Jul 8.06367	2454289.563669	16.27 ± 0.04
2007 Jul 8.07147	2454289.571465	16.27 ± 0.04

Notes.
[a] Dates are light-time corrected.
[b] Apparent magnitude.

The resulting phased B-, R- and J-band light curves of EL61 are shown in Figure 2. Two main features are immediately apparent from the light curves. Firstly, the two peaks of the light curve are unequal. The total range (peak-to-peak) is 0.29 ± 0.02 mag but the second peak is smaller by roughly 0.08 mag. This asymmetry in the light-curve peaks cannot be matched by simple equilibrium shape models of the type proposed by Rabinowitz et al. (2006), since the latter are symmetric (Chandrasekhar 1969). Secondly, we note that, in the interval roughly from 0.7 to 1.0 in rotational phase (Figure 2), the B data fall systematically below the R data. Although small, this effect appears in measurements from three different nights and hence we regard it as observationally secure. The $B - R$ color curve, computed from the data in Figure 2, is shown separately in Figure 3. There, the R magnitudes were interpolated to the rotational phases of B photometry and were subtracted from the B data points. The resulting color curve was smoothed using a running median filter to show a reddening of up to 0.035 mag. The J data are of lower signal-to-noise but, in the region near the 0.75 rotational phase, $R - J$ is also redder than near the 0.25 rotational phase peak (Figure 2).

We quantitatively assess the significance of the red feature in the $B - R$ color curve by noting that, in the interval from 0.7 to 1.0 in rotational phase, 21 of the 23 consecutive phased measurements fall above the median $B - R$ for EL61. The probability of this result is the same as the probability of obtaining at least 21 "tails" in 23 tosses of an unbiased coin.

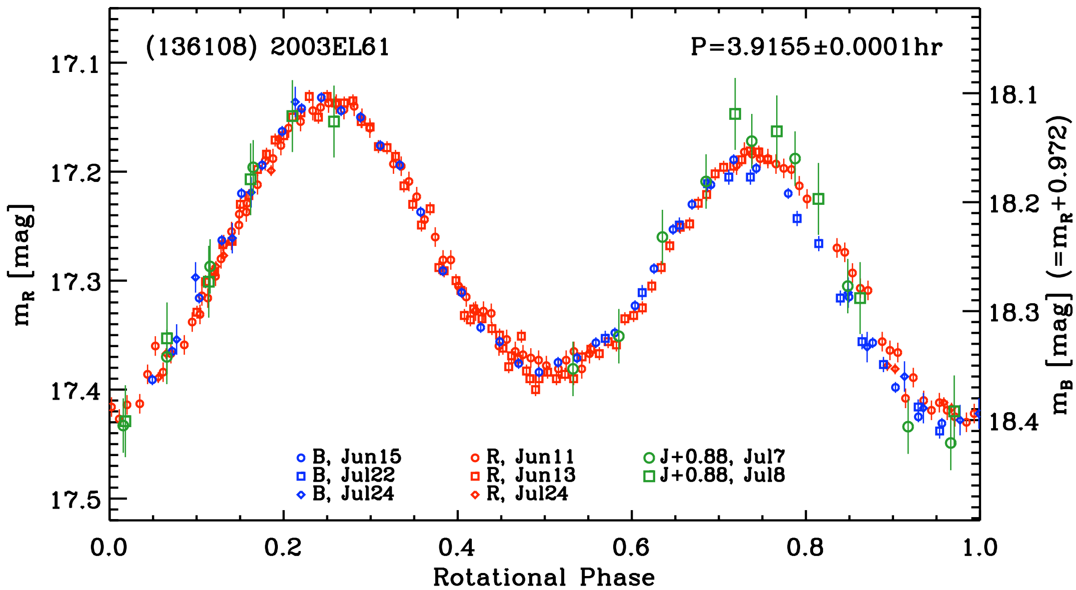

Figure 2. Light curves of EL61 through the B-, R-, and J-band. B and J data were scaled to the R data by subtracting the median colors $V - R = 0.972$ and $R - J = 0.88$. The error bars are $\sim$0.01 mag in the B and R bands, and $\sim$0.03 mag in the J band.

Table 5
Ratio of Flux Densities at 1.6 μm and 1.25 μm

UT date[a]	Julian date[a]	$f_{1.6}/f_{1.25}$[b]
2007 Jul 6.94315	2454288.443153	0.71 ± 0.04
2007 Jul 6.95097	2454288.450974	0.69 ± 0.04
2007 Jul 6.95881	2454288.458810	0.67 ± 0.03
2007 Jul 6.97424	2454288.474241	0.68 ± 0.02
2007 Jul 6.98283	2454288.482830	0.68 ± 0.02
2007 Jul 6.99100	2454288.490998	0.67 ± 0.02
2007 Jul 6.99918	2454288.499178	0.69 ± 0.02
2007 Jul 7.00775	2454288.507750	0.69 ± 0.02
2007 Jul 7.01586	2454288.515861	0.68 ± 0.02
2007 Jul 7.02574	2454288.525740	0.67 ± 0.02
2007 Jul 7.03704	2454288.537044	0.65 ± 0.02
2007 Jul 7.04504	2454288.545039	0.64 ± 0.02
2007 Jul 7.05309	2454288.553091	0.64 ± 0.02
2007 Jul 7.06125	2454288.561255	0.62 ± 0.02
2007 Jul 7.06936	2454288.569363	0.64 ± 0.02
2007 Jul 7.07745	2454288.577448	0.66 ± 0.02
2007 Jul 6.93925	2454288.439254	0.69 ± 0.04
2007 Jul 6.94707	2454288.447075	0.71 ± 0.04
2007 Jul 6.95489	2454288.454894	0.67 ± 0.03
2007 Jul 6.97032	2454288.470325	0.69 ± 0.02
2007 Jul 6.97888	2454288.478877	0.68 ± 0.02
2007 Jul 6.98708	2454288.487075	0.67 ± 0.02
2007 Jul 6.99527	2454288.495273	0.68 ± 0.02
2007 Jul 7.00384	2454288.503841	0.69 ± 0.02
2007 Jul 7.01194	2454288.511938	0.68 ± 0.02
2007 Jul 7.02182	2454288.521819	0.67 ± 0.02
2007 Jul 7.03314	2454288.533136	0.66 ± 0.02
2007 Jul 7.04112	2454288.541120	0.63 ± 0.02
2007 Jul 7.04918	2454288.549176	0.66 ± 0.02
2007 Jul 7.05733	2454288.557332	0.63 ± 0.02
2007 Jul 7.06544	2454288.565437	0.63 ± 0.02
2007 Jul 7.07356	2454288.573560	0.65 ± 0.02
2007 Jul 7.08179	2454288.581790	0.68 ± 0.02

Notes.
[a] Dates are light-time corrected.
[b] Ratio of the flux density at 1.6 μm to the flux density at 1.25 μm.

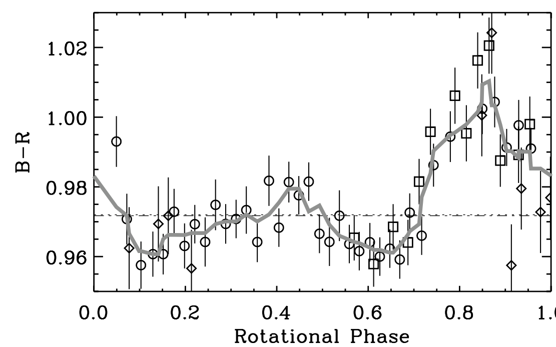

Figure 3. Circles, squares, and diamonds mark the difference between the B data and R data interpolated at the B rotational phases. Different symbols indicate different nights. A running median (width = 6) is overplotted as a thick gray line. Horizontal dotted and dot-dashed lines respectively mark the mean and median color. The reddening in the region from 0.70 to 1.05 in rotational phase is clear.

Assuming a binomial distribution, this probability is roughly $p = 3.3 \times 10^{-5}$, corresponding to $\sim 4\sigma$. Furthermore, at least nine measurements in that same interval lie $>3\sigma$ above the median, corresponding to $\sqrt{9} \times 3\sigma = 9\sigma$. In this sense, the redder region in Figure 3 is unlikely to be due to chance. This, plus the fact that the red spot is confirmed by observations on different nights together, strongly suggest that the feature is real.

Light-curve asymmetry of the type observed in Figure 2 could be caused by strength-supported topography. However, the associated color variations (Figure 3) cannot be so explained. Instead, the data are best explained by the presence of wavelength-dependent albedo markings on the surface of EL61, perhaps analogous to those already mapped on Pluto. Specifically, given that the body shape of EL61 is close to a figure of equilibrium, the multi-wavelength light-curve data show the existence of a region, near the second peak in Figure 4, that is darker and redder than elsewhere. For want of a better label, we refer to this as the "dark red spot" (DRS).

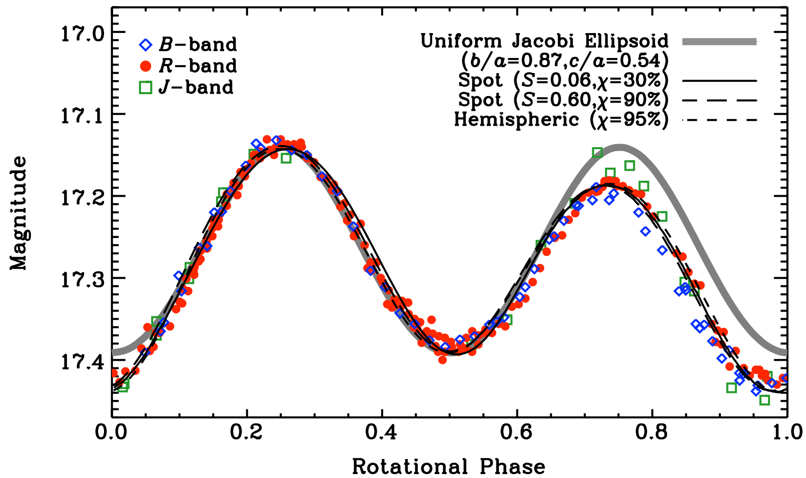

Figure 4 B, R, and J light curves of EL61 with four models overplotted. The thick grey line corresponds to a Jacobi equilibrium ellipsoid model (axis ratios $b/a = 0.87$ and $c/a = 0.54$), assumed to have uniform surface optical properties. The three thin black lines correspond to models with non-uniform surfaces. "Spot" models have darker circular regions located on the equator of the Jacobi ellipsoid, leading a semi-major axis by 45°. The numbers in parenthesis indicate the area (S, relative to the maximum cross-section of the ellipsoid, πac) and albedo (χ, relative to the surrounding regions) of the spot. In "Hemispheric," the darker region covers a whole hemisphere of EL61.

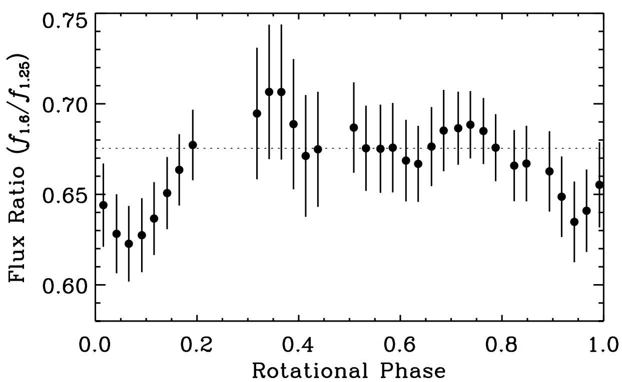

Figure 5 The ratio of the flux density at 1.6 μm to the continuum flux density at 1.25 μm measured on UT 2007 July 07. A thin horizontal dotted line marks the median of the data points. See the text for details.

The time-resolved measurements of the 1.5 μm water-ice band from UT 2007 July 07 are plotted in Figure 5. The data provide no compelling indication of variability, except that the ratio of the 1.6 μm flux density to the continuum flux density at 1.25 μm appears lower (the water-ice band deepens) near phase ∼0 than at other phases. An attempt to repeat the 1.6 μm photometry on UT 2007 July 08 was thwarted by unstable atmospheric opacity. In the absence of confirming data from a second night, we regard the variation seen in Figure 5 as interesting but inconclusive. We cannot determine whether the water-band depth varies with the rotation of EL61.

What constraints can be set on the albedo markings present on the surface of EL61? We first address the spatial extent of the DRS. In principle, the DRS could be very small compared to the instantaneous projected cross-section of EL61, but would then need to be very red and very dark relative to the surroundings in order to give rise to the observed light-curve differences. At the other extreme, the DRS could be large, possibly even hemispheric in extent, in which case its albedo and color contrast relative to the surroundings would be minimal (see Figure 6). To explore the range of possibilities we computed models in which the area of the surface of EL61 occupied by the DRS was taken as a free parameter.

The models we used are described in detail in Lacerda & Jewitt (2007). In short, we render three-dimensional models of EL61 at different rotational phases which are used to generate the synthetic light curve. In this paper we adopt a Lambert scattering law, appropriate for high-albedo icy surfaces. The spot was simulated as a region of different reflectivity and color curves were generated by subtracting the light curves of two spots of equal sizes but different reflectivities. The shape of EL61 was modeled by a Jacobi ellipsoid with axis ratios $b/a = 0.87$ and $c/a = 0.54$, which provides the best match to the light-curve data if no albedo variegation is present (see Figure 4). The size of the spot is parameterized by its sky-plane cross-section area relative to the maximum cross-section of the Jacobi ellipsoid, πac. We assumed that the rotation axis of EL61 was inclined relative to the line-of-sight by 90°, consistent with the large measured rotational light-curve range, and that the DRS is located on the equator of EL61. The observed sequence of brighter and fainter extrema indicates that the longitude of the DRS must lie in a leading quadrant with respect to one of the semi-major axes. This prediction is corroborated by our models, which further show that a longitudinal separation of 45°between the DRS and the long axis of EL61 produces a better match to the data than 30° or 60°. The ability to fit the shape of the light curves in different filters was used as a metric for the models. Three of the best-fit examples are shown in Figures 4 and 6.

The results, which confirm the qualitative expectations outlined above, are shown in Figure 7. Figure 8 combines the color and albedo constraints and allows comparison with real surfaces. Also marked in Figure 8 are the ranges of color and albedo for established outer solar system materials, including the dark regions on Pluto and Saturn's satellite Iapetus. The EL61 data are incompatible with very small patches of dark, red matter like that found on the low-albedo side of Iapetus, or even with the darker material on the surface of Pluto. Indeed, if the spot is to have a $B - R$ color within the range observed for solar system objects ($B - R \lesssim 2$), then it must be larger than ∼20% of the maximum cross-section of EL61 (see Figure 7). Instead, Iapetus' and Pluto's bright areas match the DRS in term of albedo and $B - R$ color. The surfaces of Eris (a large KBO) and 2005 FY9 are also consistent with the DRS, even if these objects have

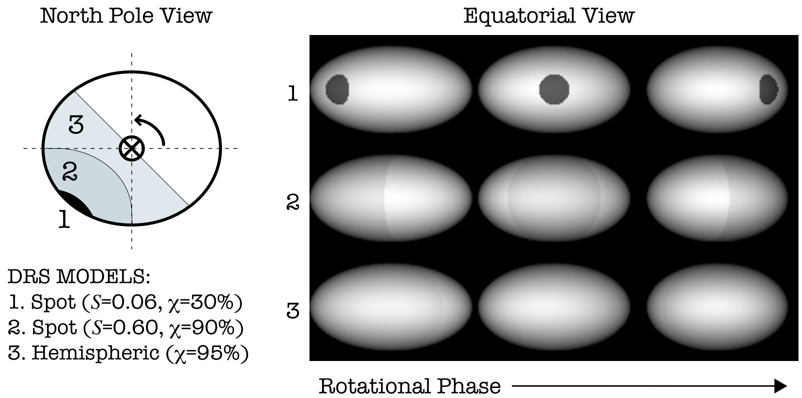

Figure 6 Sample spot models used to fit the light-curve data of EL61 in Figure 4. The north pole and three equatorial views of the ellipsoid (from left to right: flank-on, spot-on, and tip-on, or rotational phases ∼0.750, ∼0.875, and ∼1.000 in Figure 4) are shown. The spot in each model is characterized by a surface area S (expressed as a fraction of the maximum equatorial cross-sectional area of EL61) and an albedo, χ, normalized to the albedo of the surface outside the spot. The spots are assumed to be located on the equator of EL61 and leading a semi-major axis by 45°. "Hemispheric" is a model in which a whole hemisphere of EL61 has a darker albedo. The albedo ratio $\chi = 95\%$ in the hemispheric model (3) is almost imperceptible. See the text for details.

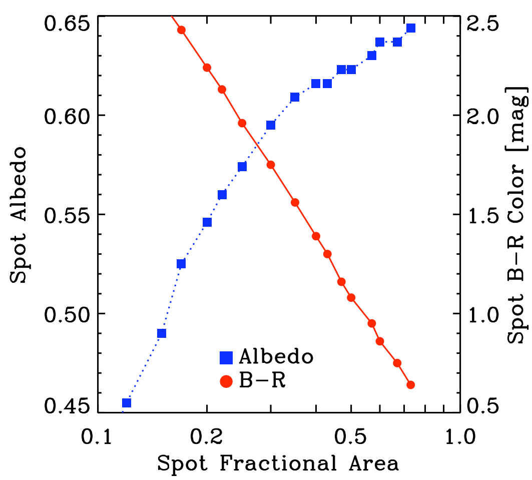

Figure 7. Range of models consistent with the light-curve data. Plotted on the left vertical axis is the assumed albedo of the spot material (the average geometric albedo of EL61 is $p = 0.70$) while on the right vertical axis we plot the assumed $B - R$ color index of the spot. The horizontal axis shows the area of the spot (as a fraction of the maximum projected cross-section of the best-fit equilibrium figure, πac.)

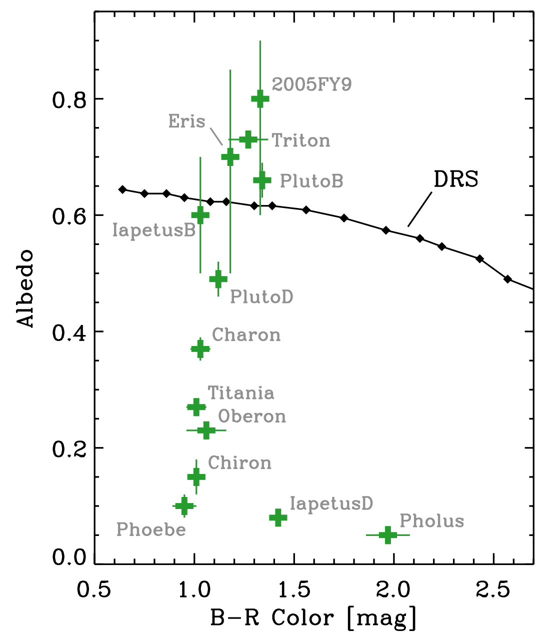

Figure 8. Combined constraints from Figure 7 on the albedo and $B - R$ color of the DRS. Overplotted are the albedo, color pairs of identified outer solar system surface types. For Iapetus and Pluto, objects with large albedo contrasts, the labels B and D correspond to the bright and dark areas, respectively.

highly uncertain albedos (Stansberry et al. 2008). All matching surface types would imply a DRS size of 35% to 50%.

Another possibility is that the DRS is simply terrain contaminated by dirt. This would account for both the darkening and the reddening, but the suspected deepening of the 1.5 μm water band close to the DRS in rotational phase (see Figure 5) would be harder to explain; a weaker, i.e. less deep, water feature would be expected if that were the case. Alternatively, the DRS could be a region depleted in a spectrally neutral substance, both brighter and bluer than water ice. A more contrived explanation involves the presence of larger water-ice grains on the DRS which would lower the albedo and redden the surface (Clark 1982), and produce deeper water-ice absorption bands (Clark 1981). On Enceladus, larger grains are found on the region often referred to as the "tiger stripes," where cryovolcanism is thought to occur (Jaumann et al. 2008).

What might be the origin of the DRS? On Pluto, the light and dark albedo markings may be self-sustaining and caused by the mobility of surface volatiles, partly driven by the seasons (Hansen & Paige 1996). There, dark regions are heated by the Sun leading to higher sublimation rates and the migration of volatiles toward brighter, cooler regions. In this way the volatile ices may naturally migrate to the restricted regions of the surface. The dominant volatile species on Pluto is the highly volatile solid nitrogen, N_2, with methane (CH_4) mixed in as an optically active tracer. In contrast, the surface of EL61 appears to be water-ice dominated, with no evidence for the diagnostic N_2 band at 2.15 μm (Figure 1). Water ice is utterly refractory at the ∼30 K temperatures on EL61, and this albedo instability mechanism seems unlikely to apply. It has been suggested that EL61 is the source of an impact-produced dynamical family of water-rich KBOs. It is tempting to speculate that the DRS could mark the scar of the impact from which the family members were purportedly excavated, although such an explanation could hardly be unique.

4. SUMMARY

From time-resolved, high-precision, optical and near-infared photometry of KBO 2003 EL_{61} we find the following results.

1. The R-band light curve has period 3.9155 ± 0.0001 h and peak-to-peak range 0.29 ± 0.02 mag. However, successive light-curve peaks in the R-band data are clearly unequal. The $B - R$ and $R - J$ colors of EL61 also vary with rotational phase.
2. No variation in the 1.5 μm water-ice band with rotational phase larger than $\sim$5% is observed in our data.
3. The observed light-curve variations are broadly consistent with a rotational equilibrium (strengthless body) model but with the additional requirement that the surface must support wavelength-dependent albedo variations ("spots") in order to explain the color variations.
4. We explored the range of parameters of possible surface spots that are consistent with the time-resolved photometry. Very small "spots" having albedo and color very different from the surroundings are ruled out by our data. Instead, the surface feature responsible for the wavelength dependence of the light curve must have an areal extent corresponding to a significant fraction of the instantaneous projected cross-section.

We thank Roy Gal and Toshi Kasuga for allowing us to observe during their scheduled time. Andrew Wang, Colin Aspin, and John Dvorak provided invaluable support. We appreciate comments from Jan Kleyna. P.L. was supported by a grant to D.J. from the National Science Foundation and N.P. by the Fundação para a Ciência e a Tecnologia, BPD/2004/18729, and by a grant to D.J. from the NASA Origins program.

REFERENCES

Buie, M. W., Tholen, D. J., & Horne, K. 1992, Icarus, 97, 211
Brown, M. E., Barkume, K. M., Ragozzine, D., & Schaller, E. L. 2007, Nature, 446, 294
Chandrasekhar, S. 1969, in Ellipsoidal Figures of Equilibrium (The Silliman Foundation Lectures) (New Haven, CT: Yale Univ. Press)
Clark, R. N. 1981, J. Geophys. Res., 86, 3087
Clark, R. N. 1982, Icarus, 49, 244
Hansen, C. J., & Paige, D. A. 1996, Icarus, 120, 247
Jaumann, R., et al. 2008, Icarus, 193, 407
Jewitt, D. C., & Luu, J. 2004, Nature, 432, 731
Jewitt, D. C., & Sheppard, S. S. 2002, AJ, 123, 2110
Lacerda, P., & Jewitt, D. C. 2007, AJ, 133, 1393
Lacerda, P., & Luu, J. 2006, AJ, 131, 2314
Landolt, A. U. 1992, AJ, 104, 340
McKinnon, W. B. 1989, ApJ, 344, L41
Persson, S. E., Murphy, D. C., Krzeminski, W., Roth, M., & Rieke, M. J. 1998, AJ, 116, 2475
Rabinowitz, D. L., Barkume, K., Brown, M. E., Roe, H., Schwartz, M., Tourtellotte, S., & Trujillo, C. 2006, ApJ, 639, 1238
Rabinowitz, D. L., Schaefer, B. E., & Tourtellotte, S. W. 2007, AJ, 133, 26
Ragozzine, D., & Brown, M. E. 2007, AJ, 134, 2160
Sheppard, S. S. 2007, AJ, 134, 787
Sheppard, S. S., & Jewitt, D. 2004, AJ, 127, 3023
Stansberry, J., Grundy, W., Brown, M., Cruikshank, D., Spencer, J., Trilling, D., & Margot, J.-L. 2008, in The Solar System Beyond Neptune, ed. M. A. Barucci, H. Boehnhardt, D. P. Cruikshank, & A. Morbidelli (Tucson, AZ: Univ. Arizona Press), 161–179
Stellingwerf, R. F. 1978, ApJ, 224, 953
Takahashi, S., & Ip, W.-H. 2004, PASJ, 56, 1099
Tegler, S. C., Grundy, W. M., Romanishin, W., Consolmagno, G. J., Mogren, K., & Vilas, F. 2007, AJ, 133, 526
Trafton, L. M. 1989, Geophys. Res. Lett., 16, 1213
Trujillo, C. A., Brown, M. E., Barkume, K. M., Schaller, E. L., & Rabinowitz, D. L. 2007, ApJ, 655, 1172
Young, E. F., Galdamez, K., Buie, M. W., Binzel, R. P., & Tholen, D. J. 1999, AJ, 117, 1063